THE JOURNAL OF PHYSICAL CHEMISTRY C

Article

Cite This: J. Phys. Chem. C 2017, 121, 23564-23573

pubs.acs.org/JPCC

Collision and Oxidation of Silver Nanoparticles on a Gold Nanoband Electrode

Fan Zhang,[†] Martin A. Edwards,[‡] Rui Hao,[†] Henry S. White,*[,‡] and Bo Zhang*[,†]

[†]Department of Chemistry, University of Washington, Seattle, Washington 98195-1700, United States

[‡]Department of Chemistry, University of Utah, Salt Lake City, Utah 84102, United States

Supporting Information

ABSTRACT: We report the use of gold nanoband electrodes ranging from 60 to 180 nm in width to study collision and oxidation of single Ag nanoparticles (NPs). The use of nanoscale electrodes has enabled the observation of unique single-NP collision responses indicating a strong electrode size effect when the critical dimension of the electrode (the bandwidth) is reduced to that of NPs. In addition to multipeak events, NP collision on a nanoband electrode displays reduced collision frequency, significantly higher probability of single-peak events, and fewer subpeaks. More importantly, the average charge transferred in a single-peak event is about 50% less than that of the first subpeak of a multipeak event. The reduced charge of single-peak collisions and the more frequent appearance on nanoelectrodes are strong evidence that NPs start to behave differently at the electrode/solution interface when the size of the electrode is reduced to be comparable to that of the NPs. The reduced charge is likely due to a weaker particle−electrode interaction when the particle collides on the edge of the nanoband electrode. Random walk numerical simulation was used to further understand the electrode size effect in single-particle collision and oxidation. The simulated results are in good agreement with the experiments. A detailed analysis of the collision signal reveals that a Ag NP is more likely to diffuse away after making its initial contact with a nanoband electrode, due to the electrode's smaller critical dimension and a possible strong edge effect from the negatively charged silicon nitride/oxide. This study offers a deeper insight into the dynamic collision behavior of metal NPs on the electrode surface.

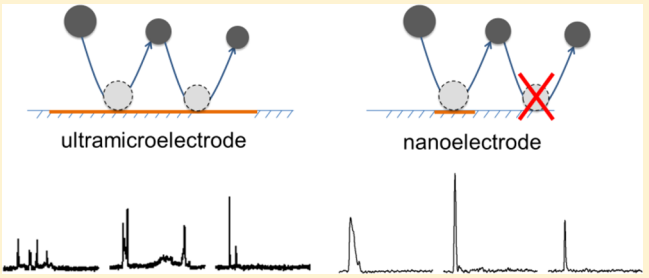

INTRODUCTION

The field of single-nanoparticle (NP) electrochemistry has grown considerably since Quinn et al.[1] and Bard and co-workers[2,3] reported their seminal work on stochastic NP collisions on an ultramicroelectrode (UME). This field of research is driven primarily by several key motivations, including the use of the transient faradaic signal to analyze particle size,[4] electrocatalytic activity,[5,6] or photoelectrochemistry of single NPs,[7,8] the use of single particles to build new sensors for biomolecules,[9−12] and the study of fundamental electrochemistry of single NPs.[13,14]

Compared with methods based on scanning electrochemical microscopy (SECM)[15,16] or optical imaging,[17,18] stochastic single-NP collision amperometry has high temporal resolution and sensitivity and is the method of choice for many single-NP studies. Depending on the problems of interest, several general strategies can be used. First, one can detect transient current decays when inert NPs are adsorbed on an UME blocking the diffusion of redox species on the electrode surface.[1,19,20] Second, a current enhancement can be expected when a NP collides on an electrocatalytically inert electrode, and the enhancement can either be based on the particle catalyzing a redox reaction[2,3,21] or the NP itself being oxidized or reduced.[4,22−24] These methods all have high sensitivity when the right combination of particles, redox reactions, and electrodes are employed leading to detection of single NPs below 5 nm in size.[6,25] The methods have now been extended to the study of single small molecules.[26−28]

A metal NP, such as silver, can be oxidized when it collides on the UME surface resulting in a sharp current spike whose charge reflects the amount of the metal oxidized during the collision. Under certain conditions, e.g., small particle size or in the presence of certain anions, the entire particle can be fully oxidized leading to an effective method for particle size analysis.[4,29] Recently, we and others have reported the observation of multiple subpeaks in the current response upon the collision of single Ag NPs with gold and carbon microelectrodes.[29−31] A typical particle collision event displays a large anodic current spike followed by several smaller subpeaks, contrasting with single peaks or steps reported for other collisions. This phenomenon was explained by the repeated collision and partial oxidation of the same NP at the electrode/solution interface.[29,30] Using particles of different sizes, the Unwin group verified that this multipeak collision and partial oxidation behavior is more significant on large particles and weaker on small ones.[29] When Ag particles are smaller than 20 nm in diameter, they tend to be completely oxidized in one

Received: August 25, 2017
Published: October 3, 2017

DOI: 10.1021/acs.jpcc.7b08492
J. Phys. Chem. C 2017, 121, 23564−23573

collision, whereas for larger particles, multipeaks caused by repeated collision and partial oxidation are dominate.

In our previous work we proposed a scheme by which a particle is oxidized in a stepwise manner as illustrated in Scheme 1a and briefly summarized as follows: (1) a Ag particle

Scheme 1. Single-NP Collision on an Ultramicroelectrode (a) versus a Nanoelectrode (b)

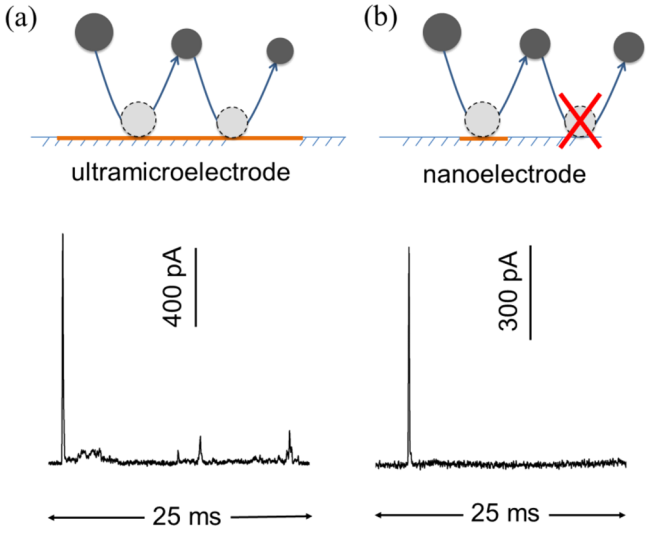

freely diffuses when it is far from the UME surface, e.g., >20 nm for a 10 mM salt concentration; (2) electrostatic interaction can attract or repel a charged NP when it moves sufficiently close to the electrode; (3) prior to a collision event, the negatively charged NP is attracted toward the positive electrode leading to particle collision and Ag dissolution; (4) the NP−electrode contact changes the surface charge of the particle from negative to positive, and the remaining NP is quickly repelled from the electrode; (5) further dissolution of Ag and readsorption of citrate ions restores the negative surface charge of the NP; (6) Brownian motion carries the remaining NP either toward the electrode leading to another subcollision or away from the UME leading to the end of the collision process.

The proposed mechanism was supported by control experiments and a numerical simulation of particle motion near the electrode surface. The experiments reported in the previous work were performed with electrodes greater than 12 μm, which limits the information one can acquire about the nanoscale motion of the particles. In this work we extend our studies to particles colliding on nanometer-scale electrodes. The insights into the nanoscale dynamics these experiments offer are shown schematically in Scheme 1b. If the multipeak response was truly caused by repeated particle collision with the same electrode, the chance of the remaining NP diffusing around and finding the same electrode would be greatly reduced when the critical dimension of the electrode is comparable to the diameter of the NP, and the proportion of the multipeak events would diminish on nanoelectrodes.

Here we characterized the collisions of Ag NPs of 66 and 40 nm with gold nanoelectrodes with critical dimensions below 200 nm. Preliminary measurements using laser-pulled gold and Pt disk nanoelectrodes (diameter ~100 nm) displayed very low particle detection frequency (<1 event/3 min). However, they did show that most of the collision events are single-peak events. Performing measurements employing gold nanoband electrodes with bandwidth between 60 and 180 nm and lengths ~80 μm delivered increased collision frequencies allowing us to collect hundreds of particle collision events. Our results demonstrated that, when the size of the NPs is comparable to the critical dimension of the electrode, i.e., the width of a nanoband electrode, an increased proportion of the collision events (40−55%) are single-peak events as compared to the 12.7 μm UME (~20%). The average number of subpeaks in a collision event on the nanoband electrode is ~50% less than that on the UME. More importantly, we find that the average charge transferred in a single-peak event is significantly less than that in the first subpeak of a multipeak event. These results suggest that the electrochemical response of single-particle collision can be strongly dependent on electrode size and how a particle interacts with the electrode when the critical dimension of the electrode is reduced to the nanoscale. We believe that such single-peak events are generated from particles making their initial collision contact near the edge of the nanoband electrode resulting in a somewhat weaker particle−electrode interaction than when they collide on the center of the electrode. Numerical simulation was used to further study single-particle collision and oxidation, and the results closely match the experimental observations.

EXPERIMENTAL SECTION AND NUMERICAL SIMULATION

Chemicals and Solutions. Silver nitrate ($AgNO_3$), trisodium citrate, potassium nitrate (KNO_3), ferrocenemethanol (FcMeOH), and sodium sulfate (Na_2SO_4) were all used as received from Sigma-Aldrich. Ultrapure water (>18 MΩ·cm) was obtained through a Barnstead Nanopure water purification system and used for all aqueous solutions. The 66 nm Ag NPs used in collision experiments were prepared in-house by citrate reduction following previous work[30] (see Supporting Information, section S2, Figure S1, for more information on NP characterization). The 40 nm Ag NPs were purchased from Nanocomposix.

The solutions for NP collision experiments were prepared by combining the stock NP solution, 100 mM KNO_3, and 10 mM trisodium citrate in a 2:1:3 ratio by volume, resulting in an approximate NP concentration of 40 pM (66 nm) or 30 pM (40 nm) and concentrations of 18 mM KNO_3 and 7 mM trisodium citrate. Solutions of both particles were found to give stable NP recording over 1 h with unchanged frequency and amplitude.

Electrode Fabrication and Characterization. To fabricate gold nanoband electrodes, quartz substrates (University Wafer) were cleaned by sonication in DI water and isopropyl alcohol and dried by a flow of nitrogen. Metals and Si_3N_4 were deposited layer by layer on the cleaned substrate. A 5 nm Cr adhesion layer was first deposited, followed by a layer of gold and another layer of 5 nm Cr that were deposited sequentially at 0.4 Å/s by a homemade thermal evaporator. The thickness of gold was varied between 50 and 170 nm to form the nanoband electrode. Subsequently, 200 nm of Si_3N_4 was deposited as an insulating layer using a plasma-enhanced chemical vapor deposition (PECVD) system with a slow deposition rate (0.6 Å/s) and low temperature (125 °C). The final focused ion beam (FIB) milling step was performed inside an FEI XL830 dual-beam system with an optimized milling current of 1 nA to create the gold nanoband electrode by milling individual 5 × 5 μm^2 square pores of ~1.5 μm deep. Scanning electron microscopy (SEM) and cyclic voltammetry (CV) were further

DOI: 10.1021/acs.jpcc.7b08492
J. Phys. Chem. C 2017, 121, 23564−23573

employed to characterize the nanoband electrodes to ensure they were properly fabricated.[32,33] A 12.7 μm diameter Au disk electrode was used as the working electrode in UME experiments.[30] Before Ag NP collision experiments, the UME was first polished by a sandpaper, and then polished in a 50 nm Al_2O_3 NPs slurry, before being finally sonicated in ultrapure water for 20 s.

Electrochemical Measurements. NP collisions were recorded using an Axopatch 200B patch-clamp amplifier (Molecular Devices) interfaced to a PC through a Digidata 1440A digitizer (Molecular Devices). The Axopatch was used in V-clamp mode with whole cell $\beta = 0.1$ and the low-pass filter set to 5 kHz. Amperometric traces were recorded with a 100 kHz sampling rate. Current spikes were analyzed using pClamp 10.4 Clampfit software (Molecular Devices). All experiments were performed using a two-electrode setup placed in a lab-built Faraday cage. A Ag/AgCl wire was used as the counter/quasi-reference electrode (QRE) in all experiments.

Numerical Simulation. Lattice random walk simulations were performed in a similar manner to those previously described in ref 30; full details are provided in the Supporting Information, section S3. Briefly, particle motion proceeded by discrete steps in time, δt, on a grid with spacing δx, with the length and duration of the steps determined from Einstein's equations for Brownian motion (eqs S1 and S2), which depended on the particle size. Initial steps for the 40/66 nm particles were 0.22/0.29 nm and 2.1/5.7 ns. Whenever the particle came in contact with the electrode a quantity of Ag was oxidized, based upon the particle surface area, the duration of the collision (δt), and the current density, J (the only free parameter). Upon oxidation the Ag particle size was changed by the amount oxidized, δt and δx were updated to reflect the new particle size, and the random walk continued. Current was calculated from the charge passed due to oxidation, which was filtered at the same rate as the experimental data. The nanoband electrode was modeled as an infinitely long band inlaid into an infinite plane (a simplification of complex microfabricated geometry), whereas the microdisk electrode was simulated as a disk in an infinite plane. Collisions with the inert support were treated as elastic with no charge transferred.

RESULTS AND DISCUSSION

Electrode Characterization. As shown in Figure 1, the Au nanoband electrode is sandwiched between a 200 nm layer of Si_3N_4 and the quartz substrate. The use of FIB milling is a simple and reproducible technique to expose the edges of the gold with the ability to control the geometry of the entire electrode. Several key parameters can be precisely controlled including the width, length, and the location of the nanoband electrode. Additionally, the use of FIB milling eliminates the need for sanding and polishing, which often results in delamination and imperfectness of the nanoband electrode.[34−36] Figure 2a displays an SEM image of a freshly milled 110 nm nanoband electrode taken at a 52° angle (see Figure S2 for electrodes of other thicknesses). The overall electrode takes a square shape with a total band length of 20 μm, which yields a reasonable amount of collision events in a 10 min recording time. Multiple nanoband electrodes can be fabricated on one device to further increase the particle detection frequency. Figure 2b is an SEM image of a 2 × 2 array of 110 nm nanoband electrodes. It is worth noting that we used devices containing single-nanoband electrodes for CV characterization and 2 × 2 nanoband arrays for particle collision.

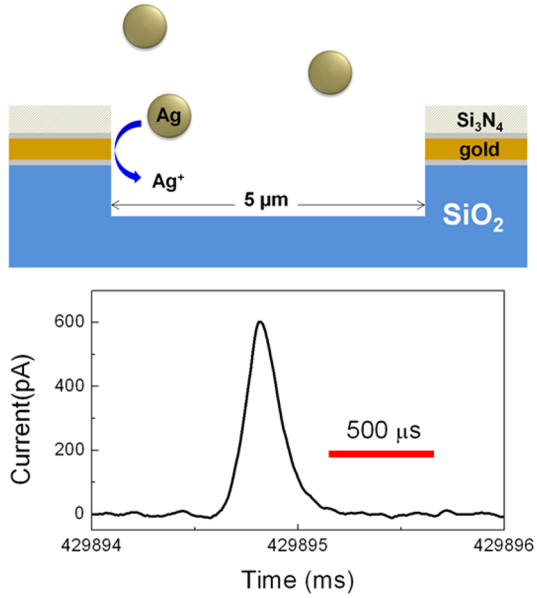

Figure 1. Top: schematic drawing of Ag NP detection on a gold nanoband electrode. Bottom: typical single-peak event detected on a gold nanoband electrode.

Single-nanoband electrodes were further characterized using cyclic voltammetry in an aqueous solution containing FcMeOH. Figure 2c shows CVs in 1 mM FcMeOH of three nanoband electrodes of different thicknesses. All electrodes show sigmoidal shape CVs typical for a nanoscale electrode (due to rapid radial diffusion). The steady-state limiting current, i_{ss}, for a nanoband electrode can be estimated from eq 1:[37]

$$i_{ss} = \frac{2\pi nFDC^*l}{\ln\left(\frac{64Dt}{w^2}\right)} \quad (1)$$

where n (n = 1 for FcMeOH) is the number of electrons transferred per redox molecule, F is the Faraday's constant (96 485 C/mol), D and C^* are the diffusion coefficient (6.7×10^{-6} cm^2/s) and concentration (mol/cm^3) of FcMeOH, l is the length of the nanoband electrode (cm), w is the bandwidth (cm) and $t = RT/F\nu$ is experimental time, where R is the gas constant (8.314 J/mol·K), T is temperature (K), and ν is the scan rate (V/s). Using eq 1, the limiting currents for the 60, 110, and 180 nm width electrodes can be estimated as 0.51, 0.56, and 0.61 nA, respectively. The measured i_{ss} for the 110 and 180 nm width electrodes are 0.52 and 0.58 nA (Figure 2c), in good agreement with the prediction.[32] The measured i_{ss} for the 60 nm width electrode (0.1 nA) is much lower than the calculated value (0.51 nA). We attribute this smaller current to possible electrode recession, which could be caused by FIB-induced melting or evaporation of the thin gold film or possible redeposition of the insulating Si_3N_4 or SiO_2 under high milling current. The shape of the CVs for all electrodes indicates that there is no apparent delamination between the metal and silicon insulators, which is the key for their successful use in Ag NP collision.

Nanoparticle Collision at Gold Nanoband Electrodes. Figure 3 shows representative traces of Ag NP detection where all the gold electrodes (a 12.7 μm disk UME and three 2 × 2 nanoband arrays) were held at +0.6 V versus Ag/AgCl. In all cases, large oxidative current spikes can be seen on top of a

DOI: 10.1021/acs.jpcc.7b08492
J. Phys. Chem. C 2017, 121, 23564−23573

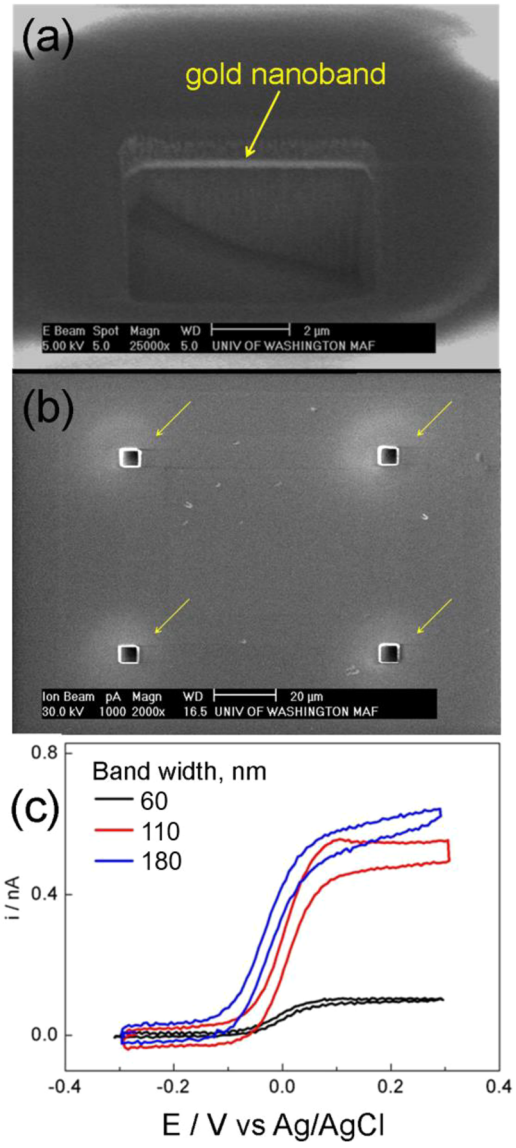

Figure 2. (a) SEM image of a 110 nm gold nanoband electrode. (b) SEM image of a 2 × 2 array of 110 nm gold nanoband electrodes. (c) CV curves at 50 mV/s of single gold nanoband electrodes with different thicknesses measured in 1 mM FcMeOH and 0.2 M Na_2SO_4.

stable baseline current indicating effective detection of particle collision events. A close inspection of the current spikes reveals several important features. First and most importantly, most (~78%) of the NP detection events collected on the disk UME contain an initial large current spike followed by several smaller subpeaks, an interesting phenomenon discovered in our previous report,[30] while for nanoband electrodes about half of the collision events display just a single peak (40−55% depending on the width of the nanoband electrode, see Table S1)! For easy comparison, we presented four of the multipeak events in the right column of Figure 3a and four typical single-peak events collected on nanoband electrodes in Figure 3b−d. The narrowest 60 nm nanoband electrode has the largest proportion of single-peak events. In addition to the drastically increased number of single-peak events, another interesting fact is that there are on average two subpeaks in each collision on the nanoband electrodes compared to 3.2 on the UME. These are exciting results indicating that the collision behavior on a nanoelectrode is quite different from the UME, which is likely due to the electrode's smaller critical dimension.

A second feature that is also dependent on the electrode's critical size is the detection frequency. The 60 nm electrode has the lowest detection frequency of 2.9 events/min. The 110 and 180 nm electrodes have similar detection frequencies of 4.8 and 5.2 events/min, respectively. As a comparison, the detection frequency on the UME is 10 events/min, which is much greater than that of the nanoband electrodes due to its larger area. We note that this frequency is lower than reported in our previous work,[30] which could be due to changes in NPs and imperfectness of the electrode surface. We also note that, despite the highly reproducible particle detection, a large variation is observed in the current amplitude of the detected events, ranging from 100 to 1000 pA. This variation probably reflects differences in the NP−electrode contact at nanoscale heterogeneity or particle-to-particle variability.[30]

To better understand this interesting collision/oxidation behavior in greater detail, we first analyzed 25 randomly selected multipeak events recorded at four different electrodes. Figure 4 shows the results of the analysis for the first four subpeaks of a multipeak event. The mean area, height, and half-width of each subpeak are plotted in Figure 4a−c, respectively, and the mean duration between subpeaks is plotted in Figure 4d. The first subpeak is the main peak with the largest peak amplitude and area, followed by several small subpeaks, and the total duration of the collision is ~20 ms. The peak height and area sharply decrease after the first subpeak and are roughly constant for subsequent subpeaks. The height and area of the first subpeak show little electrode dependence (about 500 pA and 120 fC), suggesting all electrodes perform relatively the same concerning the multipeak oxidation behavior. The half-width and interpeak spacing are about 0.2 and 4 ms on all electrodes.

The multipeak collision behavior, which is believed to be caused by repeated collision of a Ag NP on the electrode surface, was previously demonstrated by us[30] and others[29,31] on UMEs. The fact that such multipeak events are also observed on a nanoscale electrode with a critical dimension similar to the size of the NPs indicates that Ag NPs may undergo similar collision and oxidation processes as on the UME: a negatively charged particle moves near to a positive electrode and gets attracted to the electrode surface by electrostatic force giving rise to a first collision and immediate Ag oxidation, which forms the first large subpeak; the remaining particle (now at a positive potential due to charge transfer with the electrode) is repelled from the electrode followed by surface adsorption of citrate ligands; the remaining particle collides with the electrode again when/if it diffuses back forming the second subpeak; this process continues until the particle is either completely oxidized or diffuses out of the electrode/solution interface.

When an UME is used as the detection electrode, it is reasonable to assume that a significant fraction of the detected NPs collide at an area toward the center of the electrode. Therefore, the probability of the remaining particle that diffuses back finding the same electrode is relatively high, as evidenced by the ~80% multipeak events. The remaining 20% single-peak events are likely due to NPs making their initial contact toward the edge of the UME. In this case, there is a higher chance that the remaining particle would not collide back on the electrode when it diffuses around. This situation is greatly exaggerated when a nanoband electrode is used, where the effective electrode area for a second collision is greatly reduced when the

DOI: 10.1021/acs.jpcc.7b08492
J. Phys. Chem. C 2017, 121, 23564−23573

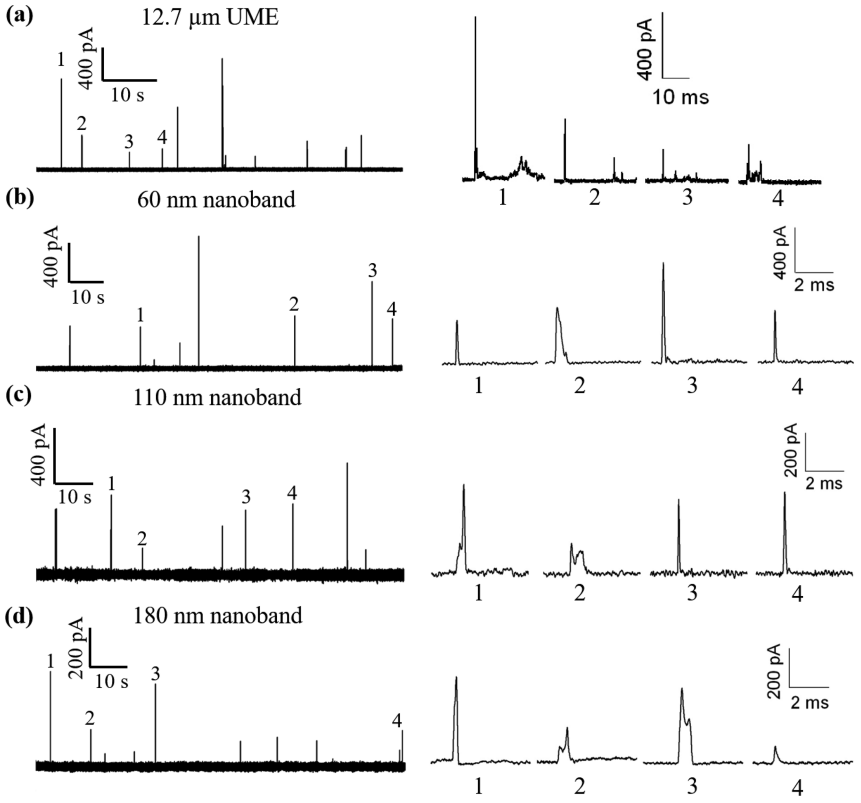

Figure 3. Representative current−time traces of 66 nm Ag NPs at a 12.7 μm Au UME (a) and Au nanoband electrodes of different thicknesses: (b) 60, (c) 110, and (d) 180 nm. Right column shows details of representative peaks. Conditions: 40 pM Ag NPs, 7 mM trisodium citrate, 18 mM potassium nitrate, and oxidation potential of 0.6 V.

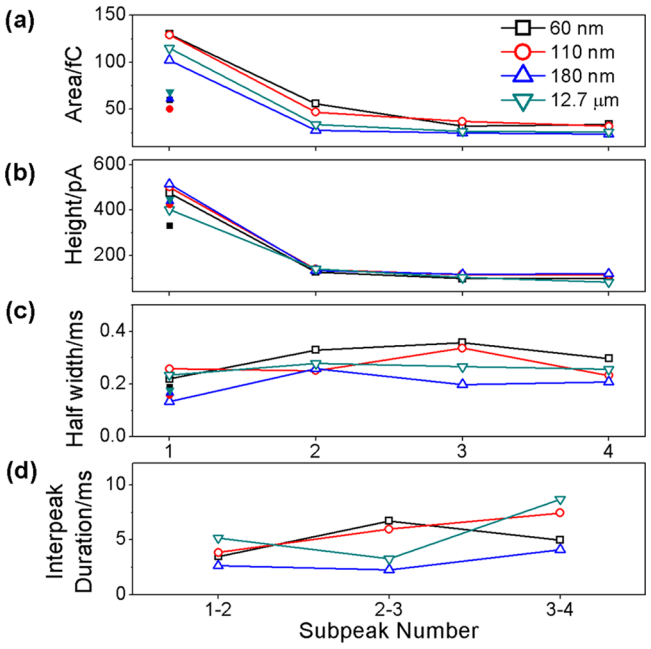

Figure 4. Analysis of the first four subpeaks for 25 randomly selected multipeak events recorded at different detection electrodes. (a−c) Mean subpeak area, height, and half-width, respectively. (d) Mean interpeak spacing. Solid dots in panels a−c represent values of single-peak events at different electrodes. Conditions: 40 pM Ag NPs (66 nm diameter), 7 mM trisodium citrate, 18 mM potassium nitrate, and oxidation potential of 0.6 V.

remaining particle diffuses around the narrow band. We believe this is the main factor leading to the higher probability of observing single-peak collisions. Detailed characterizations of single-peak events are summarized in Table 1. The peak height, area, and half-width are estimated to be 400 pA, 60 fC, and 0.17 ms. Considering the large standard deviation (SD), all electrodes have the same single-peak characteristics regardless of their bandwidth based on data in Table 1.

Influence of Applied Potential. We have found that the probability of observing single-peak collision events on gold electrodes does not depend on the applied potential when the potential is altered from 0.6 to 0.8 V. Table S1 shows that the proportion of single-peak events for all electrodes at different potentials. Nanoband electrodes still have a greatly increased probability of observing single peaks. Several key parameters of multipeak and single-peak events, such as peak height, half-width, and peak area, are summarized in Figure 5 and Table 1. Here, we use the 180 nm nanoband electrode as an example for multipeak statistics. Results for other electrodes are shown in Figure S3. A weak potential dependence is observed on peak amplitude and area suggesting that increasing potential above 0.6 V does not lead to further oxidation of Ag NPs. Importantly, the average peak height and area of single-peak events are lower than that of the first peak of the multipeak events at almost all potentials. For example, the average peak area of 65 fC is only ∼55% of the first peak in a multipeak event. This is a very interesting result because it could indicate that the single-peak and multipeak events are due to completely different particle−electrode interactions. The smaller peak amplitude and charge of single-peak events may indicate that they are due to particles colliding on the edge of the Au

DOI: 10.1021/acs.jpcc.7b08492
J. Phys. Chem. C 2017, 121, 23564−23573

Table 1. Statistics for Single-Peak Events of 66 nm Ag NPs on Different Electrodes and Potentials[a]

electrode type	potential/V	peak height/pA	SD peak height/pA	half-width/ms	SD half-width/ms	Q/fC	SD Q/fC
60 nm band	0.6	330	219	0.19	0.13	59	42
	0.7	348	277	0.14	0.04	59	54
	0.8	351	243	0.14	0.06	63	56
110 nm band	0.6	422	332	0.15	0.08	50	39
	0.7	333	204	0.16	0.09	64	40
	0.8	305	172	0.19	0.1	74	42
180 nm band	0.6	440	256	0.16	0.06	60	44
	0.7	489	258	0.14	0.06	60	49
	0.8	423	313	0.19	0.13	69	71
12.7 μm diameter UME	0.6	447	191	0.17	0.08	67	42
	0.7	324	113	0.19	0.06	53	21
	0.8	321	123	0.18	0.09	60	50

[a]A total of 35 single peaks are randomly selected for nanoband electrodes and 15 single peaks for microelectrodes.

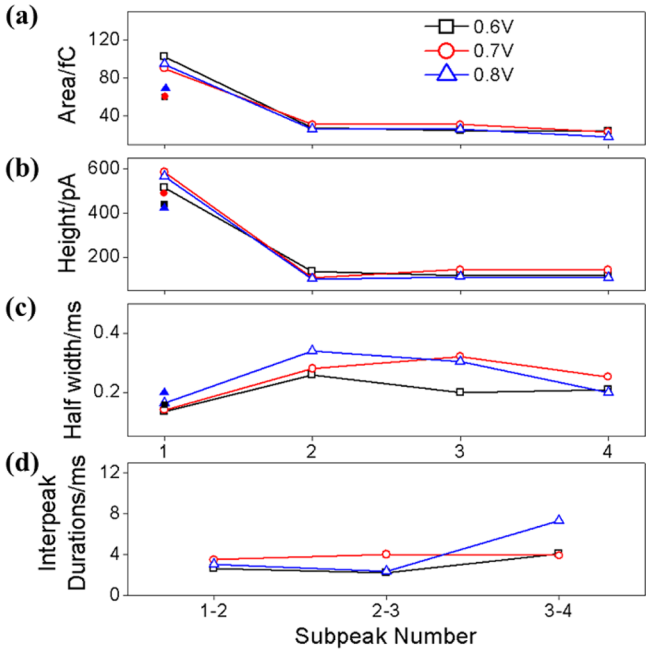

Figure 5. Analysis of the first four subpeaks for 25 randomly selected multipeak events recorded on the 180 nm nanoband electrode at different potentials. (a–c) Mean subpeak area, height, and half-width, respectively. (d) Mean interpeak spacing. Solid dots in panels a–c represent values of single-peak events at different potentials. Conditions: 40 pM Ag NPs (66 nm diameter), 7 mM trisodium citrate, 18 mM potassium nitrate.

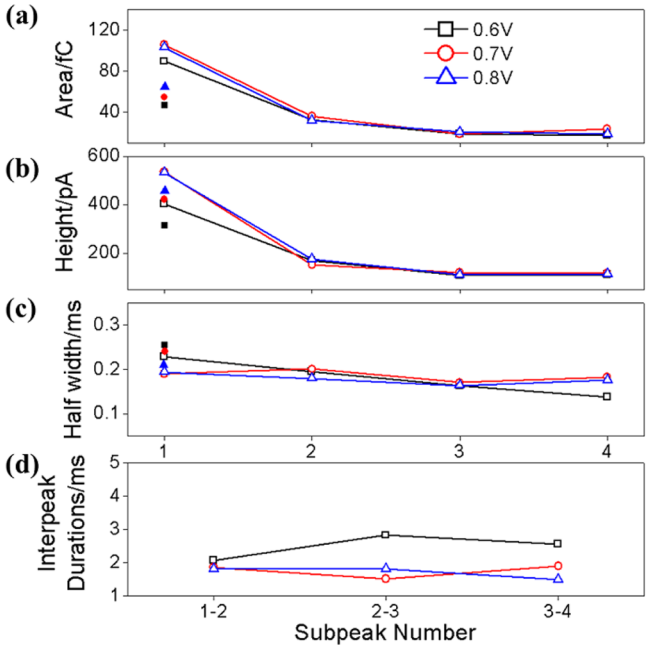

Figure 6. Analysis of the first four subpeaks for 25 randomly selected multipeak events recorded on the 180 nm nanoband electrode at different potentials. (a–c) Mean subpeak area, height, and half-width, respectively. (d) Mean interpeak spacing. Solid dots in panels a–c represent values of single-peak events at different potentials. Conditions: 30 pM Ag NPs (40 nm diameter), 7 mM trisodium citrate, 18 mM potassium nitrate.

nanoband electrode and the negative NPs are more strongly affected (repelled) by the negative charges on the SiO_2 and Si_3N_4.[38,39] A simple calculation shows that the 65 fC charge in these single-peak collision events corresponds to oxidation of only ~5% of a 66 nm Ag NP, implying Ag NPs quickly diffuse away after a somewhat weak contact with the electrode.

A parameter that is potential-dependent is the detection frequency, especially seen on the 60 and 110 nm nanoband electrodes (Table S1). Interestingly, a 50% enhancement in detection frequency is observed at 0.8 V than at 0.6 V. This phenomenon is drastically different from a gold UME, where the detection frequency is constant and is probably diffusion-controlled.[19] The exact reason to the frequency enhancement is unclear at this moment. However, it may be partially due to the slightly recessed geometry of the nanoband electrode or the use of a thin 200 nm silicon nitride film, which may induce a stronger electrostatic effect in attracting particles toward the electrode at higher potentials. Another possible reason is that the nanoband electrodes may have higher electrocatalytic activity toward Ag oxidation at higher potentials leading to more detectable collisions.

Effect of Particle Size. To further examine single-NP collision behavior on NPs of other sizes, we performed collision experiment using 40 nm Ag NPs, and the key results are summarized in Table S2. The overall collision behavior of 40 nm Ag NPs is quite similar to the 66 nm NPs. First, the probability of observing single-peak events increases as the width of the nanoband electrode decreases regardless of the applied potential. Second, the detection frequency increases drastically at higher potentials, a phenomenon observed on all nanoband electrodes. Different from the 66 nm NPs, the 180 nm nanoband electrode shows obvious potential dependence

DOI: 10.1021/acs.jpcc.7b08492
J. Phys. Chem. C 2017, 121, 23564–23573

Table 2. Statistics for Single-Peak Events of 40 nm Ag NPs on Different Electrodes and Potentials[a]

electrode type	potential/V	peak height/pA	SD peak height/pA	half-width/ms	SD half-width/ms	Q/fC	SD Q/fC
60 nm band	0.6	292	131	0.17	0.05	46	39
	0.7	345	216	0.23	0.13	54	28
	0.8	332	214	0.18	0.06	55	31
110 nm band	0.6	354	186	0.17	0.07	47	32
	0.7	344	145	0.17	0.08	54	19
	0.8	331	177	0.23	0.14	57	18
180 nm band	0.6	313	187	0.25	0.16	46	35
	0.7	420	232	0.23	0.15	55	34
	0.8	455	297	0.2	0.11	65	45
12.7 μm diameter UME	0.6	277	132	0.26	0.13	51	29
	0.7	401	165	0.16	0.05	59	16
	0.8	350	165	0.17	0.07	60	17

[a]A total of 35 single peaks are randomly selected for nanoband electrodes and 20 single peaks for microelectrodes.

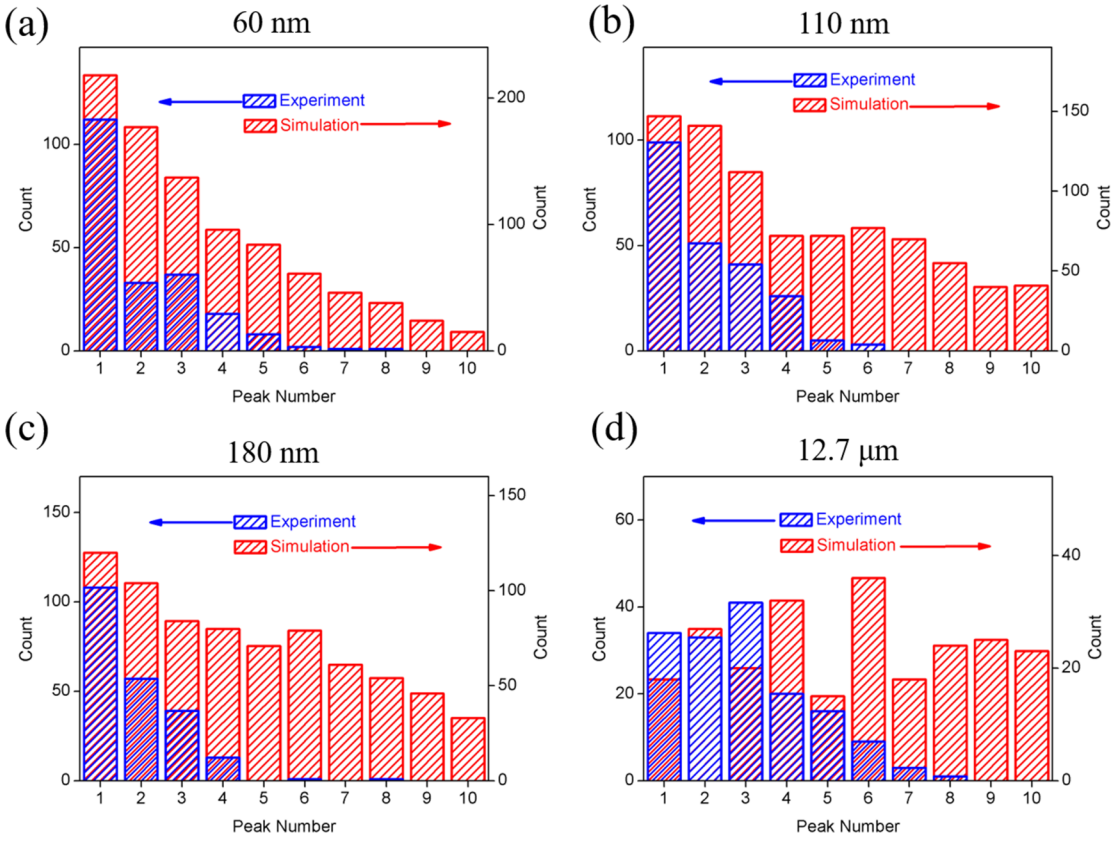

Figure 7. Histograms of peak number for oxidation of 66 nm Ag NPs on different electrodes at 0.6 V: (a) 60 nm nanoband electrode; (b) 110 nm nanoband electrode; (c) 180 nm nanoband electrode; (d) 12.7 μm UME. Only values from 1 to 10 are shown.

for 40 nm Ag NPs: the detection frequency increased from 6.2 events/min at 0.6 V to 13.5 events/min at 0.8 V, implying that electrocatalytic or electrostatic effects are strong enough to oxidize more 40 nm Ag NPs.

Figure 6 shows parameters of 25 randomly selected multipeak events collected from the 180 nm nanoband electrode at three potentials. Data from other electrodes are shown in Figure S4. The first peak in a multipeak event has a height of 400−500 pA and transferred charge of ~100 fC. The average half-width and interpeak spacing are ~0.2 and 2 ms, respectively. Compared to the summary from 66 nm Ag NPs (Figure 5), little difference can be extracted. Parameters for all single-peak events are given in Table 2. The transferred charge is ~50 fC corresponding to 15% oxidation of a 40 nm Ag NP, which is higher than the 5% oxidation on the 66 nm Ag NPs, and the trend is in agreement with recent results of Unwin's group.[29]

Importantly, the transferred charge of a single-peak event is again ~50% smaller than that of the first peak of a multipeak event. This is in agreement with the results from the 66 nm particles, and the results support out hypothesis that particle−electrode interaction in a single-peak event is likely near the edge of the nanoband electrode. Considering the significant difference in charge and peak amplitude between single-peak and multipeak events, we believe that we are starting to capture some of the exciting size effects of heterogeneous electron-transfer reactions when the size of the redox species approaches the critical dimension of the electrode as previously suggested

DOI: 10.1021/acs.jpcc.7b08492
J. Phys. Chem. C 2017, 121, 23564−23573

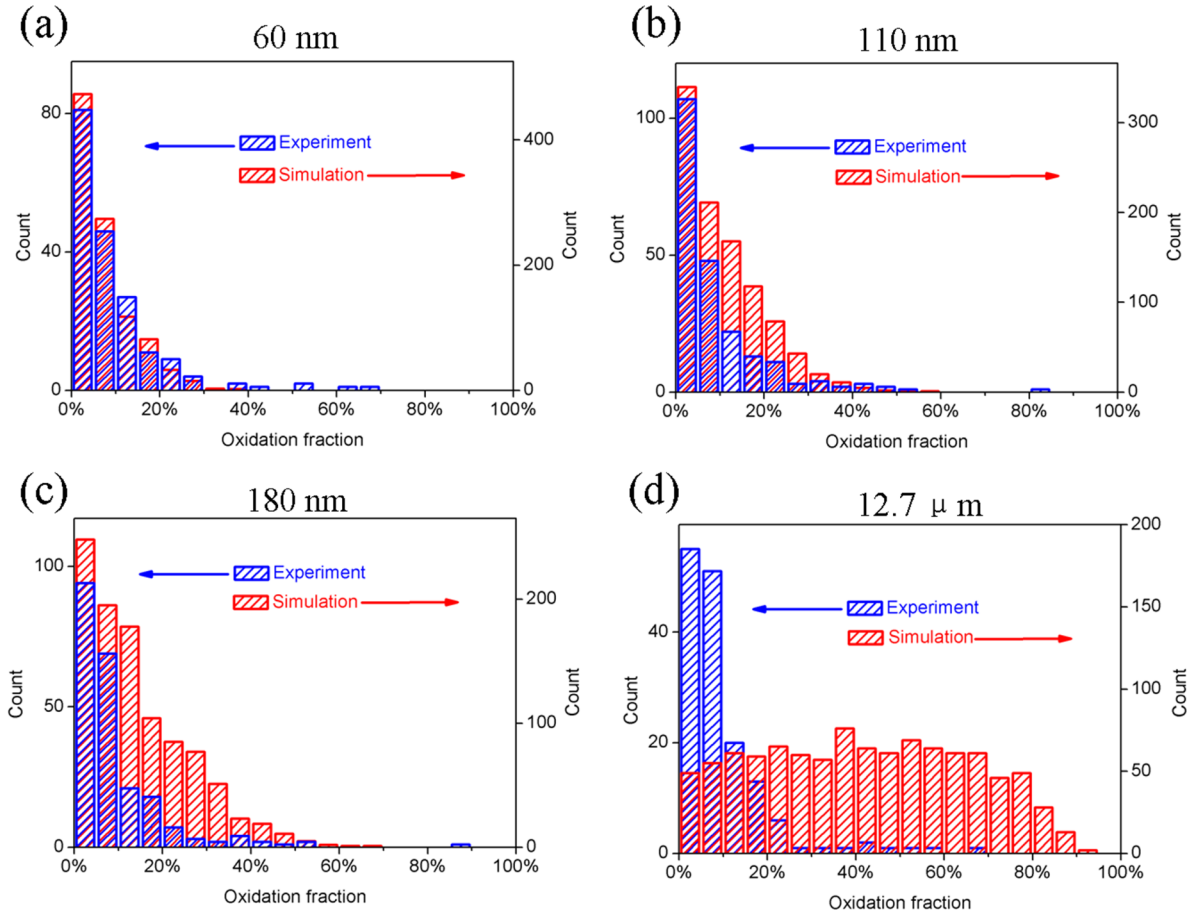

Figure 8. Histograms of oxidation fraction during one collision event (66 nm Ag NPs on different electrodes at 0.6 V): (a) 60 nm nanoband electrode; (b) 110 nm nanoband electrode; (c) 180 nm nanoband electrode; (d) 12.7 μm UME.

by Morris et al.[40] Despite that the redox-active species are individual Ag NPs, their size is close or slightly smaller than the width of the nanoband electrode. One can imagine that the electron-transfer kinetics between such a large particle and the gold could be dependent on where and how the particle interacts with the nanoband electrode: a weaker interaction may be expected when the particle initially lands on the edge of the nanoband electrode resulting in slower electron-transfer kinetics and reduced charge; a stronger interaction may be expected when the particle touches the middle of the nanoband electrode giving rise to faster electron transfer and more transferred charge. Another important factor to consider is the negative charges on the insulating walls[41] (silicon nitride or silicon oxide), which also reduce the effectiveness of particle−electrode interaction because the particles are negatively charged prior to collision.

Numerical Simulation. The Ag NPs collision behavior on electrodes was further studied and verified by lattice random walk simulation, a method previously reported by White.[42] Simulation details are close to experimental conditions. The Ag NP diameters were chosen to be 66 and 40 nm despite the real NPs coming from a wide distribution. For the band electrode, the actual simulated widths are 60, 110, and 180 nm because of an additional 10 nm Cr layer in each electrode. To simplify the calculation, infinite band length was applied. The only adjustable parameter, current density for Ag NP oxidation, was set to be 500 A/cm^2 for both 66 and 40 nm NPs. Only one particle was simulated at one time by starting at a random position on the electrode surface at t = 0. Then, the particle collision produces oxidation spikes similar to experimental amperometric traces (Figure S5), which have been post filtered at 5 kHz to make a direct comparison with the experiment.

A summary of simulated peak number for all electrodes is shown in Figure 7, together with experimental values. Here, results for 66 nm NP are shown and that for 40 nm NP is included in the Supporting Information. It is clear that, for all nanoband electrodes, more single-peak events (number of subpeaks = 1) are observed than for the 12.7 μm UME. For example, among 970 effective collision events on a 60 nm band electrode, at least 218 are definitely single peaks (22%), whereas on the UME, this ratio sharply decreases to ∼2%. And the NP tends to collide many times on the UME during oxidation, which matches well with experiment. Here noise-free traces make it easier to distinguish more subpeaks in simulation. As a result, more collision events are attributed as multipeak events (red bars). However, the difference of percentage of single-peak events still strongly confirms the electrode size effect on NP collision.

Oxidation fractions for simulation and experiment are shown in Figure 8. Simulated results show that, for a 60 nm nanoband electrode, the dominating oxidation fraction is about 5% during one collision event, similar to experimental values. When the bandwidth is increased to 180 nm, slightly higher oxidation ratio is observed (Figure 8a−c). When the 12.7 μm gold UME is applied, the distribution of oxidation fraction tends to be uniform for all values (Figure 8d). Higher average oxidation

DOI: 10.1021/acs.jpcc.7b08492
J. Phys. Chem. C 2017, 121, 23564−23573

ratio is explained by more collision times of NPs on a larger electrode. The experiment summary (blue bars) matches with simulation prediction. For the UME, although events with oxidation ratio below 5% account for the largest proportion, those with 10% oxidation cannot be ignored, which is quite different from the nanoband electrodes. As summarized previously, simulation reproduces partial oxidation for almost all collision events, suggesting the quick diffusion nature of NPs during one collision event. And in experiment, it is highly possible that the NP movement at the electrode surface is driven by Brownian motion. A simple calculation shows that a 66 nm Ag NP can move 60 nm within 0.3 ms [$D = 6 \times 10^{-8}$ cm^2/s, diffusion length = $(2Dt)^{1/2}$]. As a result, it is reasonable to expect a NP can easily escape from a nanoband electrode after its first contact with the electrode, producing fewer multipeak events than on an UME. The theory is further supported by simulation on 40 nm NPs, whose details can be found in Figures S6 and S7.

CONCLUSIONS

In summary, gold nanoband electrodes with a critical dimension ranging from 60 to 180 nm have been fabricated and used to study single-particle collision and oxidation of Ag NPs. Nanoband electrodes were prepared by thin-film deposition and FIB milling to expose the metal electrodes. Electrochemical recording of single-NP collision was carried out using 66 and 40 nm silver NPs. In addition to the observation of multipeak collision behavior, our results on nanoband electrodes have shown unique NP collision behavior indicative of a strong electrode size effect. Interestingly, we found that about half of the collision events are short single-peak events on a nanoband electrode compared to ∼20% on a 12.7 μm UME. More importantly, the charge transferred in a single-peak event is significantly less than that in the first subpeak of a multipeak event. These results suggest that the particle−electrode interaction in a single-peak collision is somewhat weaker than in a multipeak collision. Such single-peak events are probably from particles making their initial collision near the edge of the nanoband electrode. Numerical simulation was used to help understand the experiments, and the simulated results were found to closely match the experimental observations. The reduction of multipeak behavior at nanoband electrodes is supported by lattice random walk methods. Detailed analysis of experiment and simulation demonstrates that a Ag NP is easier to diffuse away after making an initial contact with a nanoband electrode due to the electrode's smaller critical dimension and a possible strong edge effect from the negatively charged silicon nitride/oxide. This study offers a deeper insight into the dynamic behavior of metal NPs on the electrode surface.

ASSOCIATED CONTENT

Supporting Information

The Supporting Information is available free of charge on the ACS Publications website at DOI: 10.1021/acs.jpcc.7b08492.

Summary of 66 and 40 nm Ag NP collisions at different electrodes and oxidation potentials, TEM characterization, description of lattice random walk simulations, SEM images of nanoband electrodes, potential-dependent multipeak analysis, typical simulated $i-t$ traces, and summary of peak number and oxidation fraction for 40 nm NPs on different electrodes (PDF)

AUTHOR INFORMATION

Corresponding Authors

*E-mail: white@chem.utah.edu.
*E-mail: zhangb@uw.edu.

ORCID

Henry S. White: 0000-0002-5053-0996
Bo Zhang: 0000-0002-1737-1241

Notes

The authors declare no competing financial interest.

ACKNOWLEDGMENTS

This research was supported by AFOSR MURI (FA9550-14-1-0003). Part of this work was conducted at the Molecular Analysis Facility, a National Nanotechnology Coordinated Infrastructure site at the University of Washington which is supported in part by the National Science Foundation (Grant ECC-1542101), the University of Washington, the Molecular Engineering and Sciences Institute, the Clean Energy Institute, and the National Institutes of Health. The authors also thank C. Han for TEM imaging, and C. G. Gunderson and Z. Wang for providing the assistance in PECVD fabrication and amperometry measurement at the University of Washington.

REFERENCES

(1) Quinn, B. M.; van't Hof, P. G.; Lemay, S. G. Time-Resolved Electrochemical Detection of Discrete Adsorption Events. *J. Am. Chem. Soc.* **2004**, *126*, 8360−8361.

(2) Xiao, X.; Bard, A. J. Observing Single Nanoparticle Collisions at an Ultramicroelectrode by Electrocatalytic Amplification. *J. Am. Chem. Soc.* **2007**, *129*, 9610−9612.

(3) Xiao, X.; Fan, F.-R. F.; Zhou, J.; Bard, A. J. Current Transients in Single Nanoparticle Collision Events. *J. Am. Chem. Soc.* **2008**, *130*, 16669−16677.

(4) Zhou, Y.-G.; Rees, N. V.; Compton, R. G. The Electrochemical Detection and Characterization of Silver Nanoparticles in Aqueous Solution. *Angew. Chem. Int. Ed.* **2011**, *50*, 4219−4221.

(5) Kleijn, S. E. F.; Lai, S. C. S.; Miller, T. S.; Yanson, A. I.; Koper, M. T. M.; Unwin, P. R. Landing and Catalytic Characterization of Individual Nanoparticles on Electrode Surfaces. *J. Am. Chem. Soc.* **2012**, *134*, 18558−18561.

(6) Guo, Z.; Percival, S. J.; Zhang, B. Chemically Resolved Transient Collision Events of Single Electrocatalytic Nanoparticles. *J. Am. Chem. Soc.* **2014**, *136*, 8879−8882.

(7) Brasiliense, V.; Patel, A. N.; Martinez-Marrades, A.; Shi, J.; Chen, Y.; Combellas, C.; Tessier, G.; Kanoufi, F. Correlated Electrochemical and Optical Detection Reveals the Chemical Reactivity of Individual Silver Nanoparticles. *J. Am. Chem. Soc.* **2016**, *138*, 3478−3483.

(8) Fernando, A.; Parajuli, S.; Alpuche-Aviles, M. A. Observation of Individual Semiconducting Nanoparticle Collisions by Stochastic Photoelectrochemical Currents. *J. Am. Chem. Soc.* **2013**, *135*, 10894−10897.

(9) Stewart, M. E.; Anderton, C. R.; Thompson, L. B.; Maria, J.; Gray, S. K.; Rogers, J. A.; Nuzzo, R. G. Nanostructured Plasmonic Sensors. *Chem. Rev.* **2008**, *108*, 494−521.

(10) Saha, K.; Agasti, S. S.; Kim, C.; Li, X.; Rotello, V. M. Gold Nanoparticles in Chemical and Biological Sensing. *Chem. Rev.* **2012**, *112*, 2739−2779.

(11) Dick, J. E.; Renault, C.; Bard, A. J. Observation of Single-Protein and DNA Macromolecule Collisions on Ultramicroelectrodes. *J. Am. Chem. Soc.* **2015**, *137*, 8376−8379.

(12) Dick, J. E.; Hilterbrand, A. T.; Strawsine, L. M.; Upton, J. W.; Bard, A. J. Enzymatically Enhanced Collisions on Ultramicroelectrodes for Specific and Rapid Detection of Individual Viruses. *Proc. Natl. Acad. Sci. U. S. A.* **2016**, *113*, 6403−6408.

DOI: 10.1021/acs.jpcc.7b08492
J. Phys. Chem. C 2017, 121, 23564−23573

(13) Kleijn, S. E. F.; Lai, S. C. S.; Koper, M. T. M.; Unwin, P. R. Electrochemistry of Nanoparticles. *Angew. Chem. Int. Ed.* **2014**, *53*, 3558−3586.
(14) Oja, S. M.; Fan, Y.; Armstrong, C. M.; Defnet, P.; Zhang, B. Nanoscale Electrochemistry Revisited. *Anal. Chem.* **2016**, *88*, 414−430.
(15) Sun, T.; Yu, Y.; Zacher, B. J.; Mirkin, M. V. Scanning Electrochemical Microscopy of Individual Catalytic Nanoparticles. *Angew. Chem. Int. Ed.* **2014**, *53*, 14120−14123.
(16) Kim, J.; Renault, C.; Nioradze, N.; Arroyo-Currás, N.; Leonard, K. C.; Bard, A. J. Electrocatalytic Activity of Individual Pt Nanoparticles Studied by Nanoscale Scanning Electrochemical Microscopy. *J. Am. Chem. Soc.* **2016**, *138*, 8560−8568.
(17) Fang, Y.; Wang, W.; Wo, X.; Luo, Y.; Yin, S.; Wang, Y.; Shan, X.; Tao, N. Plasmonic Imaging of Electrochemical Oxidation of Single Nanoparticles. *J. Am. Chem. Soc.* **2014**, *136*, 12584−12587.
(18) Nizamov, S.; Kasian, O.; Mirsky, V. M. Individual Detection and Electrochemically Assisted Identification of Adsorbed Nanoparticles by Using Surface Plasmon Microscopy. *Angew. Chem. Int. Ed.* **2016**, *55*, 7247−7251.
(19) Kwon, S. J.; Zhou, H.; Fan, F.-R. F.; Vorobyev, V.; Zhang, B.; Bard, A. J. Stochastic Electrochemistry with Electrocatalytic Nanoparticles at Inert Ultramicroelectrodes-theory and Experiments. *Phys. Chem. Chem. Phys.* **2011**, *13*, 5394−5402.
(20) Boika, A.; Thorgaard, S. N.; Bard, A. J. Monitoring the Electrophoretic Migration and Adsorption of Single Insulating Nanoparticles at Ultramicroelectrodes. *J. Phys. Chem. B* **2013**, *117*, 4371−4380.
(21) Kwon, S. J.; Bard, A. J. Analysis of Diffusion-Controlled Stochastic Events of Iridium Oxide Single Nanoparticle Collisions by Scanning Electrochemical Microscopy. *J. Am. Chem. Soc.* **2012**, *134*, 7102−7108.
(22) Ellison, J.; Tschulik, K.; Stuart, E. J. E.; Jurkschat, K.; Omanović, D.; Uhlemann, M.; Crossley, A.; Compton, R. G. Get More Out of Your Data: A New Approach to Agglomeration and Aggregation Studies Using Nanoparticle Impact Experiments. *ChemistryOpen* **2013**, *2*, 69−75.
(23) Sokolov, S. V.; Bartlett, T. R.; Fair, P.; Fletcher, S.; Compton, R. G. Femtomolar Detection of Silver Nanoparticles by Flow-Enhanced Direct-Impact Voltammetry at a Microelectrode Array. *Anal. Chem.* **2016**, *88*, 8908−8912.
(24) Hao, R.; Zhang, B. Observing Electrochemical Dealloying by Single-Nanoparticle Collision. *Anal. Chem.* **2016**, *88*, 8728−8734.
(25) Hao, R.; Fan, Y.; Zhang, B. Electrochemical Detection of Nanoparticle Collision by Reduction of Silver Chloride. *J. Electrochem. Soc.* **2016**, *163*, H3145−H3151.
(26) Alligrant, T. M.; Nettleton, E. G.; Crooks, R. M. Electrochemical Detection of Individual DNA Hybridization Events. *Lab Chip* **2013**, *13*, 349−354.
(27) Han, L.; Wang, W.; Nsabimana, J.; Yan, J.-W.; Ren, B.; Zhan, D. Single Molecular Catalysis of a Redox Enzyme on Nanoelectrodes. *Faraday Discuss.* **2016**, *193*, 133−139.
(28) Sekretaryova, A. N.; Vagin, M. Y.; Turner, A. P. F.; Eriksson, M. Electrocatalytic Currents from Single Enzyme Molecules. *J. Am. Chem. Soc.* **2016**, *138*, 2504−2507.
(29) Ustarroz, J.; Kang, M.; Bullions, E.; Unwin, P. R. Impact and Oxidation of Single Silver Nanoparticles at Electrode Surfaces: One Shot Versus Multiple Events. *Chem. Sci.* **2017**, *8*, 1841−1853.
(30) Oja, S. M.; Robinson, D. A.; Vitti, N. J.; Edwards, M. A.; Liu, Y.; White, H. S.; Zhang, B. Observation of Multipeak Collision Behavior During the Electro-Oxidation of Single Ag Nanoparticles. *J. Am. Chem. Soc.* **2017**, *139*, 708−718.
(31) Ma, W.; Ma, H.; Chen, J.-F.; Peng, Y.-Y.; Yang, Z.-Y.; Wang, H.-F.; Ying, Y.-L.; Tian, H.; Long, Y.-T. Tracking Motion Trajectories of Individual Nanoparticles Using Time-resolved Current Traces. *Chem. Sci.* **2017**, *8*, 1854−1861.
(32) Guerrette, J. P.; Percival, S. J.; Zhang, B. Voltammetric Behavior of Gold Nanotrench Electrodes. *Langmuir* **2011**, *27*, 12218−12225.
(33) Hao, R.; Zhang, B. Nanopipette-Based Electroplated Nanoelectrodes. *Anal. Chem.* **2016**, *88*, 614−620.
(34) Caston, S. L.; McCarley, R. L. Characteristics of Nanoscopic Au Band Electrodes. *J. Electroanal. Chem.* **2002**, *529*, 124−134.
(35) Lanyon, Y. H.; De Marzi, G.; Watson, Y. E.; Quinn, A. J.; Gleeson, J. P.; Redmond, G.; Arrigan, D. W. M. Fabrication of Nanopore Array Electrodes by Focused Ion Beam Milling. *Anal. Chem.* **2007**, *79*, 3048−3055.
(36) Lanyon, Y. H.; Arrigan, D. W. M. Recessed Nanoband Electrodes Fabricated by Focused Ion Beam Milling. *Sens. Actuators, B* **2007**, *121*, 341−347.
(37) Bard, A. J.; Faulkner, L. R. *Electrochemical Methods: Fundamentals and Applications*, 2nd ed.; John Wiley & Sons: New York, 2001.
(38) German, S. R.; Luo, L.; White, H. S.; Mega, T. L. Controlling Nanoparticle Dynamics in Conical Nanopores. *J. Phys. Chem. C* **2013**, *117*, 703−711.
(39) Lan, W.-J.; Holden, D. A.; Zhang, B.; White, H. S. Nanoparticle Transport in Conical-Shaped Nanopores. *Anal. Chem.* **2011**, *83*, 3840−3847.
(40) Morris, R. B.; Franta, D. J.; White, H. S. Electrochemistry at Platinum Band Electrodes of Width Approaching Molecular Dimensions: Breakdown of Transport Equations at Very Small Electrodes. *J. Phys. Chem.* **1987**, *91*, 3559−3564.
(41) Thakar, R.; Wilburn, J. P.; Baker, L. A. Studies of Edge Effects with Shroud-Modified Electrodes. *Electroanalysis* **2011**, *23*, 1543−1547.
(42) White, R. J.; White, H. S. A Random Walk Through Electron-Transfer Kinetics. *Anal. Chem.* **2005**, *77*, 214A−220A.

DOI: 10.1021/acs.jpcc.7b08492
J. Phys. Chem. C 2017, 121, 23564−23573